

Article

Powering-up Wireless Sensor Nodes Utilizing Rechargeable Batteries and an Electromagnetic Vibration Energy Harvesting System

Salar Chamanian ^{1,*}, Sajjad Baghaee ¹, Hasan Ulasan ¹, Özge Zorlu ², Haluk Külâh ^{1,2} and Elif Uysal-Biyikoglu ¹

¹ Department of Electrical and Electronics Engineering, Middle East Technical University, Ankara 06400, Turkey; E-Mails: sajjad@baghaee.com (S.B.); hulusan@metu.edu.tr (H.U.); kulah@metu.edu.tr (H.K.); uelif@metu.edu.tr (E.U.-B.)

² Middle East Technical University-Micro Electro-Mechanical Systems (METU-MEMS) Research and Applications Center, Middle East Technical University, Ankara 06400, Turkey; E-Mail: zorlu@metu.edu.tr

* Author to whom correspondence should be addressed; E-Mail: salar.chamanian@metu.edu.tr; Tel.: +90-312-210-6086; Fax: +90-312-210-2304.

External Editor: Erol Gelenbe

Received: 9 June 2014; in revised form: 29 August 2014 / Accepted: 1 September 2014 /

Published: 2 October 2014

Abstract: This paper presents a wireless sensor node (WSN) system where an electromagnetic (EM) energy harvester is utilized for charging its rechargeable batteries while the system is operational. The capability and the performance of an in-house low-frequency EM energy harvester for charging rechargeable NiMH batteries were experimentally verified in comparison to a regular battery charger. Furthermore, the power consumption of MicaZ motes, used as the WSN, was evaluated in detail for different operation conditions. The battery voltage and current were experimentally monitored during the operation of the MicaZ sensor node equipped with the EM vibration energy harvester. A compact (24.5 cm³) in-house EM energy harvester provides approximately 65 μ A charging current to the batteries when excited by 0.4 g acceleration at 7.4 Hz. It has been shown that the current demand of the MicaZ mote can be compensated for by the energy harvester for a specific low-power operation scenario, with more than a 10-fold increase in the battery lifetime. The presented results demonstrate the autonomous operation of the WSN, with the utilization of a vibration-based energy harvester.

Keywords: autonomous wireless sensor node; MicaZ; energy harvesting; electromagnetic energy harvester; rechargeable battery

1. Introduction

Wireless sensor networks (WSN) have become an important component for automation and monitoring in today's general ICT infrastructure. A WSN is established by autonomous wireless communication devices, which are equipped with several sensors, such as light, sound, temperature, humidity, acceleration, magnetic fields, *etc.* Managing the power consumption of a node in a WSN is an essential step to prop up a reliable network with a long, maintenance-free operation lifetime [1,2]. Analyses and optimization of communication systems and networks have been performed [3–6] toward the development of theoretical design principles for, as well as the demonstration of energy harvesting communication networks as part of the Energy harvesting Communication network: Optimization and demonstration (E-CROPS) project [7].

The lifetime of the communication nodes in the network are affected by the WSN architecture, environmental parameters and battery capacity. In [8], battery performance is evaluated over the WSN characteristics, such as the power consumption of the nodes and communication distance. The impacts of operating temperature, discharge current and discharging-charging cycle on the battery lifetime has been experimentally demonstrated in [9]. Utilizing energy harvesting systems as alternative energy sources is one of the most promising solutions to reduce the battery lifetime limitations and dependency of battery performance on the network characteristics and operation environment [10].

Energy harvesters exploit environmental energy sources, such as heat, sunlight, RF signals or vibration, and convert them to electrical energy. Solar energy harvesters are more interesting in outdoor applications due to the availability of sunlight [11]. However, the generated energy level scales with the size of the solar panel, and the efficiency is drastically affected for indoor applications [12]. In RF power harvesters, the challenge is the efficient design of the interface circuit with the limited RF power in the environment [13,14]. Hence, RF energy harvesting is mostly useful if there exists an RF power base station, or for powering ultra-low power wireless architectures, or a sensor network when the node operates with a very low duty cycle. Among the mentioned ambient energy sources, vibration is particularly attractive, as it is easily available in daily life, such as in vehicle motions, human movements and seismic vibrations that vary in frequency and amplitude. These vibrations are harvested by using different energy conversion methods, such as piezoelectric, electrostatic and electromagnetic (EM) transduction. The piezoelectric energy conversion is the most common approach used for harvesting vibrations in the range of 40 Hz to 400 Hz [15,16]. However, most of the vibrations lie at a lower frequency band (<20 Hz), leading to challenges in reducing the energy harvester size. Besides, the high output impedance of piezoelectric and electrostatic harvesters potentially leads to low power levels at the harvester output [17,18]. EM energy harvesters are good candidates for operation at a low frequency band due to the presence of a magnet, which naturally acts as a concentrated seismic mass, enabling the matching of the resonance frequency of the system with the ambient vibration frequency within a limited device volume [19].

Although there are plenty of theoretical works examining the limits of energy harvesting WSNs [20–23], there are only a few examples including a practical application. In [24], an RF energy harvesting system with a power combiner circuit was used to increase the primary battery lifetime of the ultra-low power node for safety monitoring of vehicle equipment. A 120-Hz, cantilever-type piezoelectric energy harvester has been presented in detail, and the operation of a custom-designed transmitter on the harvested energy with a 1.6% duty cycle has been demonstrated in [15]. A low-power sensor node for condition monitoring in [25] was autonomously powered by a meandering piezoelectric energy harvester excited with 0.45 g at 40.8 Hz. In this battery-free system, initially, the required energy was added up in a storage buffer while the system was off, and after a threshold was reached, the sensor node was turned on to read the sensors and to receive and transmit data within a determined time interval.

This study demonstrates the utilization of an electromagnetic energy harvester for charging the batteries of a MicaZ wireless sensor node while the node is operational. The energy harvester module has been designed and fabricated for energy generation at low vibration frequencies, and the MicaZ mote has been optimized for low power operation. “On-line” charging enables continuous operation of the WSN, while increasing its battery lifetime. This paper is organized as follows: A detailed description of the MicaZ architecture is presented in Section 2. Section 3 presents the utilized EM energy harvester together with its battery charging characteristics. The measurement results of the MicaZ power consumption with and without the EM energy harvester are presented in Section 4. Finally, the conclusion is given in Section 5.

2. MicaZ System Architecture and Energy Consumption Features

2.1. Hardware and Software

In this study, one of the most utilized WSN platforms, MicaZ motes from Crossbow Technology, Inc., has been used as the testbed [26]. This platform is equipped with an IEEE 802.15.4 compliant, Chipcon CC240 RF transceiver and Atmega 128L micro-controller. The MicaZ mote was equipped with MTS310CB [27] data acquisition sensor boards, containing various devices, such as a dual-axis accelerometer, a dual-axis magnetometer, light, temperature and acoustic sensors and a sounder. For this study, the accelerometer of the data acquisition sensor board was used. A gateway MicaZ mote in collaboration with a MIB520 programming board was connected to a laptop, which acts as the network fusion center.

TinyOS 2.1.0 [28], an open-source, event-based operating environment, was installed and applied as the operating system of the MicaZ motes. Eclipse IDEv3.5.0, which is equipped with the Yeti2 plugin (a TinyOS plugin), was used for generating and modifying the codes. Data processing was done in MATLAB and Microsoft Excel.

To observe the MicaZ mote current variation curve during the experiments, an Instek GDS-2072A Visual Persistence Digital Storage Oscilloscope was applied as a monitoring and recording unit. Moreover, HPVEE software ran on a PC, which was connected to a digital multimeter for recording the current and voltage variation of the batteries, and these were used during the experiments.

2.2. Energy Consumption Model and Components

One of the main determinants of reliable network operation is the node lifetime. Conserving a node's battery power and voltage as much as possible is important for many sensing applications, as variations in power supply voltage level may directly affect the sensor output [29].

By keeping track of the current consumption of a node in different operational modes and taking occasional measurements of the residual supply voltage (e.g., battery), the life time of a node can be estimated. The total energy consumption of a node within the time period $(0, T)$ can be calculated as follows:

$$E_{\text{con},i}(T) = \int_0^T V_{\text{PS}}(t) I_{\text{con},i}(t) dt \quad (1)$$

where $I_{\text{con},i}(t)$ is the instantaneous current drawn by node i and $V_{\text{PS}}(t)$ is the power supply voltage level. Equation (1) can be used for measuring the energy consumption of each unit in a WSN node, such as the micro controller unit (MCU), radio, Light Emitting Diodes (LED) and the sensors. For the rest of the presented experiments in this section, the power supply level was kept fixed at 2.6 V by using a DC power supply. Therefore, the only unknown parameter of Equation (1) becomes the current waveform, $I_{\text{con},i}(t)$ with this configuration, the current consumption of each unit of the WSN node was measured. One of these units is the microcontroller, which is the ATmega128L for MicaZ motes. This microcontroller has different operation modes, such as active, idle, extended standby, power-down, power-save, ADC noise reduction and standby. By using the TinyOS code, just the microcontroller of MicaZ was activated and set in different modes. An empty-loop application was used to put the MCU in active mode. As soon as the MCU finishes executing 10^5 empty loops, it goes to the other modes, which are defined in the TinyOS code. Therefore, current flow variations for each mode can be monitored on the oscilloscope.

There are three LEDs on the MicaZ mote. For capturing the current draw by LEDs, a code was generated to periodically activate and turn off the red LED. The transceiver unit utilized in MicaZ is CC2420, and it has only one receive (RX) mode and seven transmit modes (TX). For capturing the MicaZ RX current, one MicaZ mote (Node 1) was programmed to receive (RX) the data. All components on Node 1 and the sensor board were turned off by the TinyOS code, except the radio unit. Another MicaZ mote (Node 2) was programmed to broadcast (TX) 36 bytes of packet data. For recognizing the exact period and current consumption of RX and TX units of Node 1 and Node 2, the 36 bytes of packet data were sent six times every 2 s by Node 2. Consequently, all of the broadcasted data was detected by Node 1, without any loss. By monitoring the current values and averaging the consecutive measurement results, the accurate values of the time period and current flow were obtained for the RX and TX modes. It should be noted that the MCU is in idle mode when the radio unit sends and receives data; therefore, the idle mode current value of the MCU was deducted from the measured values. The experiment for the TX current flow measurements was done for all of the possible RF transmission power levels, ranging from 0 dBm (1 mW) to -25 dBm (seven levels) [30].

The accelerometer (ADXL202JE) on the sensor-board was selected as the data acquisition device. This device is a low-power MEMS surface micro-machined two-axis accelerometer with a dynamic range of ± 2 g and 10-bit resolution. For this study, only one axis of the sensor was activated for

measurement by the TinyOS code. Table 1 summarizes the current drawn by different units of the MicaZ mote, tested with the presented procedure.

Table 1. Average current draw of the MicaZ components.

Radio unit (mA)	MCU (mA)	Acceleration sensor	Light emitting diodes (LEDs)
TX: 0 dBm	17.2		
TX: -1 dBm	16.2		
TX: -3 dBm	15.5		
TX: -5 dBm	13.8	Active 7.8	
TX: -7 dBm	12.5	Idle 3.4	~0.5 mA 2.2 mA each
TX: -10 dBm	11	Standby 0.024	
TX: -15 dBm	10		
TX: -25 dBm	8.5		
RX	19		

2.3. MicaZ Operation Scenario

An operation scenario was setup to observe the energy consumption of each operation executed by the MicaZ mote in order to optimize the lifetime of the network and to design the energy harvester unit. According to the scenario, MicaZ was supplied with a DC supply at 2.6 V and was programmed to read the acceleration data 10 times and average the read data. The node ID plus the averaged data were broadcasted to another MicaZ mote every 1 min (the task execution period).

The RF transmission power was set to -25 dBm, which has a minimum current consumption of 8.5 mA, according to the experimental results shown in Table 1. After broadcasting the data, the transceiver was switched to the power-saving mode (standby). All of the LEDs and sensors were deactivated, except the accelerometer. Figure 1 demonstrates the transient current of the MicaZ mote for this operation scenario. The corresponding current value of each event is given in Table 2. With the help of this scenario, the average power consumption has been estimated. It is seen that the sensor read operation and the standby mode are the dominant contributors to the power dissipation for this operation scenario.

Figure 1. The current draw of the MicaZ mote with the given operation scenario.

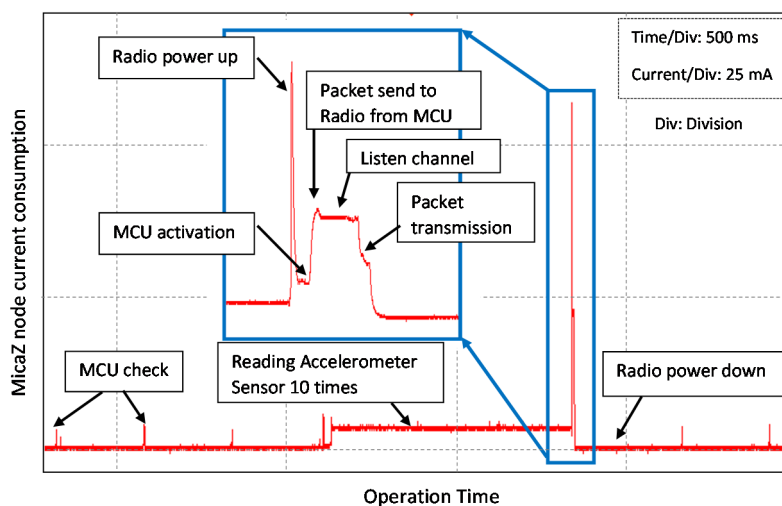


Table 2. MicaZ energy consumption for each operation (2.6 V power supply).

Event	Current draw	Duration	Energy consumption
MCU check	0.8 mA	$300 \times 760 \mu\text{s}$	474 μJ
Reading acceleration sensor (10 \times)	3.7 mA	670 ms	6.4 mJ
Radio power up	~ 60 mA	590 μs	92 μJ
MCU activation	7.8 mA	760 μs	15.41 μJ
Packet send from MCU to radio	23.8 mA	840 μs	51.97 μJ
Listen channel	22 mA	7.16 ms	410 μJ
Radio calibration and packet transmission	13.2 mA	960 μs	32.94 μJ
Standby time	24 μA	59.091 s	3.687 mJ
Total	–	60 s	11.162 mJ (186.04 μW)

3. Electromagnetic Energy Harvester

3.1. Energy Harvester Implementation

In the frame of this study, the effect of introducing an EM energy harvester into a WSN system on the charge and discharge profile of its battery was experimentally investigated. Figure 2 presents the block diagram of the implemented energy harvesting system, which is composed of a simple and low-cost in-house EM energy harvester and an interface electronic circuit. The energy harvester utilized in the presented system has been adopted from the previously reported harvesters by the authors [19,31–33] regarding the energy consumption characteristics of the MicaZ motes reported in Table 2. The utilized energy harvester module is composed of a cylindrical tube package, two fixed magnets at the upper and bottom caps, a free moving magnet suspended inside the tube and a pick-up coil, which is wound around the tube. When the energy harvester is exposed to vibration towards the tube axis, the free magnet starts moving, and an AC voltage is induced across the coil according to Faraday's law of induction. The harvested voltage is rectified and boosted with the help of a two-stage Dickson rectifier, which steps-up the input AC voltage about four times, considering that the threshold voltage drops (V_{th}) of the utilized diodes ($V_{\text{DC}} = 4 \times (V_{\text{AC,peak}} - V_{\text{th}})$). The schematic of the rectifier is presented in Figure 3. A small-sized 10- μF SMD capacitor, mounted on the PCB, is used for storing the output DC voltage.

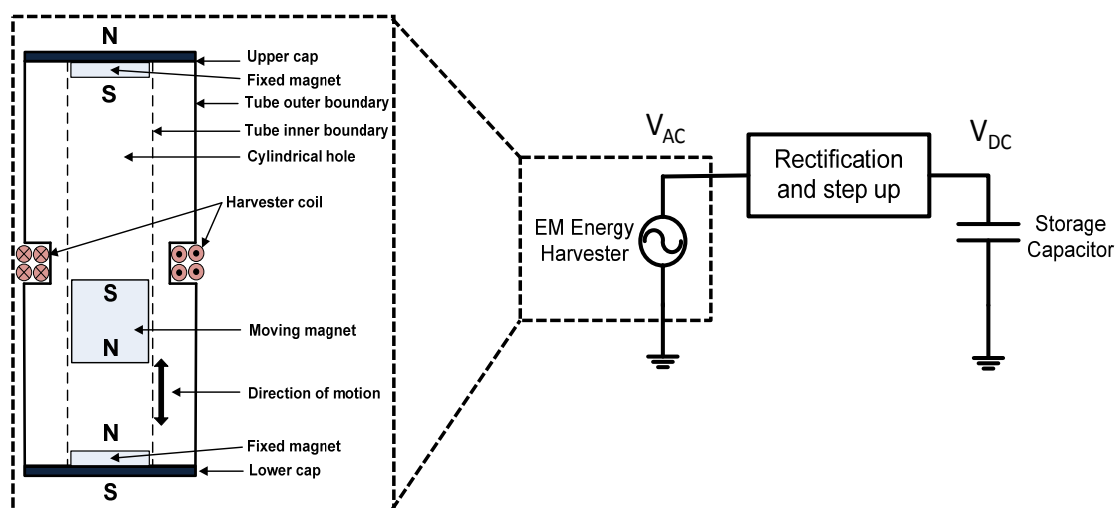
Figure 2. Block diagram of the energy harvesting system. EM, electromagnetic.

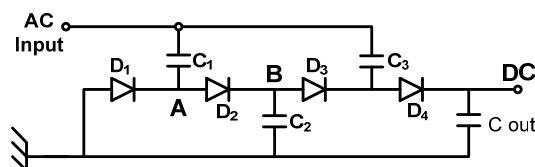
Figure 3. Schematic of the two-stage Dickson rectifier.

Figure 4 shows the assembled energy harvester module and the rectifying electronics on Printed Circuit Board (PCB). The volume of the system is 24.5 cm^3 , which is about the size of a regular C-type battery. The harvester coil wound around the tube has 1,000 turns and 185Ω internal resistance. The size of the utilized fixed magnets is $5.3 \times 5.3 \times 5.3 \text{ mm}^3$ and the moving cylindrical magnet has a 7.5-mm height and 10-mm diameter. The resonance frequency of the assembled EM energy harvester is determined by the mass of the free magnet and the force interaction between the magnets, which is related to their sizes. The location of the coil and the size of the free magnet are optimized for achieving the maximum change of the magnetic flux through the coil. The number of coil turns determines the induced voltage across the terminals; however, a compromise must be made between the internal resistance of the coil and the generated voltage to obtain a high overall efficiency. Besides, in the rectifier stage, ultra-low threshold PMEG2005EL Schottky chip diodes [34] were utilized to minimize the voltage drop during rectification. Figure 5 represents the generated RMS open-circuit output voltage across the coil for different excitation frequencies for 4-mm peak-to-peak displacement. The highest induced RMS voltage was achieved for the 7.4-Hz frequency, corresponding to 0.4 g acceleration, and the operation bandwidth (BW) of the harvesters (-3 dB bandwidth) was measured as 1.3 Hz.

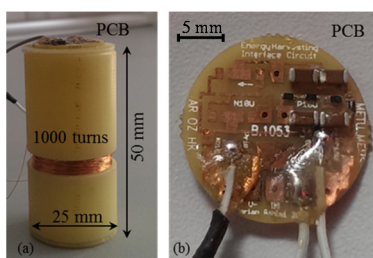
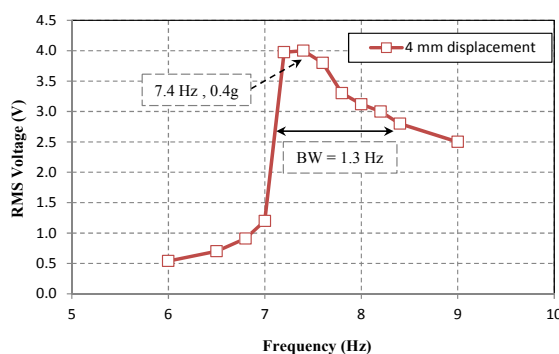
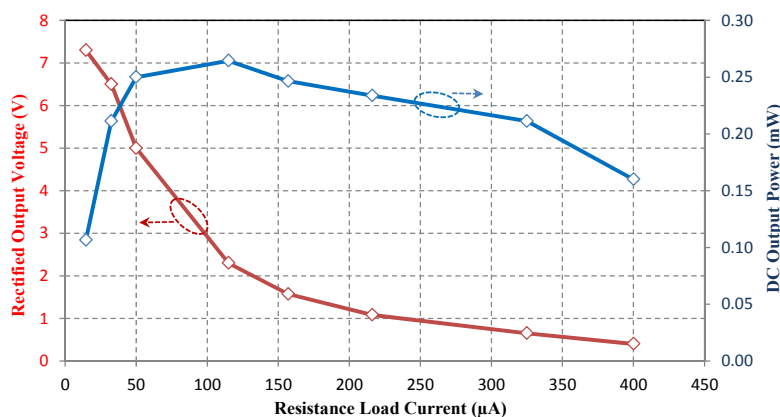
Figure 4. (a) The fabricated energy harvester module; and (b) the rectifying electronics on Printed Circuit Board (PCB).**Figure 5.** Frequency response of the fabricated EM energy harvester excited with 4-mm displacement. The RMS value of the output voltage is maximized at 7.4 Hz, corresponding to a 0.4-g peak acceleration.

Figure 6 shows the rectified output voltage and the output power as a function of the load current. The maximum power of 263 μW can be delivered to a 115 μA ($20\text{ k}\Omega$) load at an external vibration frequency of 7.4 Hz and 0.4 g.

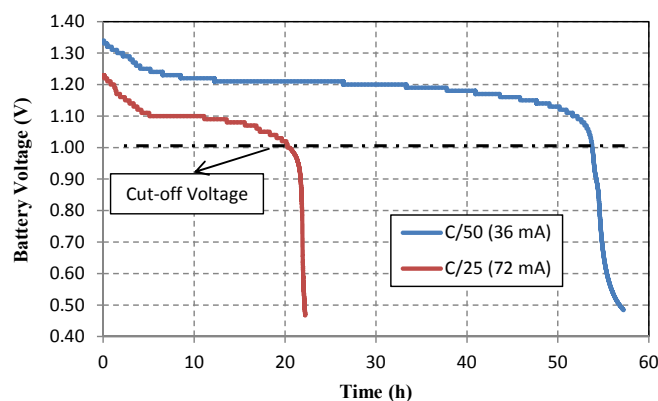
Figure 6. Characteristic of the EM energy harvesting system excited with a 7.4-Hz frequency and 0.4-g acceleration; the rectified output voltage and output power vs. load current drawn from the DC output terminal.



3.2. Charging Characteristics of NiMH Rechargeable Battery

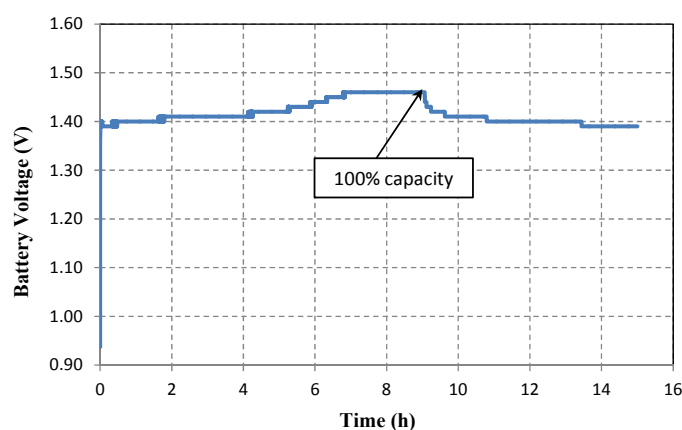
Utilization of the fabricated energy harvester for charging rechargeable batteries was studied as the next step. For this, the charging and discharging characteristics of the batteries were analyzed. The state-of-the-art rechargeable battery type on the market is the nickel metal hybrid (NiMH), with a nominal cell voltage of 1.2 V and a charged open circuit voltage ranging from 2.5 to 3.5 V [35]. Figure 7 illustrates the discharge characteristic of the 1800-mAh NiMH battery under constant current load. The value of the battery voltage is dependent on the discharge current: a higher load current results in a lower battery voltage, due to the higher voltage drops on the internal resistance of the battery. For most of the discharge time, the voltage profile remains flat at a value known as the midpoint voltage. Depending on the discharge current, the midpoint voltage may vary between 1.1 and 1.25 V. When the battery voltage falls below a certain cutoff, it drops extremely fast, and further discharging may cause damage to the cells and consequently degrade the battery capacity. As seen in Figure 7, the cutoff voltage is about 1 V for NiMH batteries.

Figure 7. NiMH discharge characteristic with a constant discharge current of 36 and 72 mA.



A NiMH cell can be charged by three different methods: fast charge (1 to 4 h), slow charge (up to 12 h) and trickle charge, which is used for keeping the battery in a fully-charged state to recover self-discharging. Figure 8 shows the charging profile of the battery from its cut-off voltage of around 1 V by a regular charger by using slow rate charging. When the battery acquires full charge (100% capacity), the charger automatically terminates the process. Here, maintaining the most efficient charge condition is critical for the battery lifetime, so the charging current and the battery temperature are regulated by the charger while charging.

Figure 8. Voltage variation of a 1800-mAh NiMH battery with slow rate charging.



To compare, the batteries were charged with the energy harvester system. For this test, two serially connected NiMH batteries are used, as they would be arranged in this configuration while powering the MicaZ mote. Figure 9 illustrates the full test setup, which consists of a shaker table, a control unit, an amplifier, a feedback accelerometer, an interface computer and a multi-meter. The energy harvester was excited in different vibration conditions, and the harvested current was continuously forced into the batteries for charging. The rechargeable batteries were charged, starting from their cut-off discharge voltage, 2 V (1 V each).

Figure 9. The test setup of charging two series rechargeable batteries.

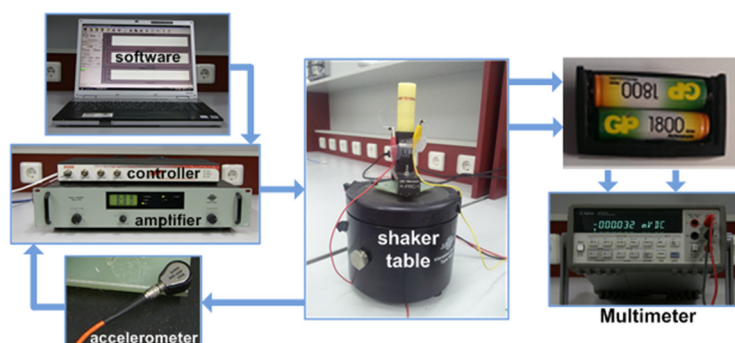
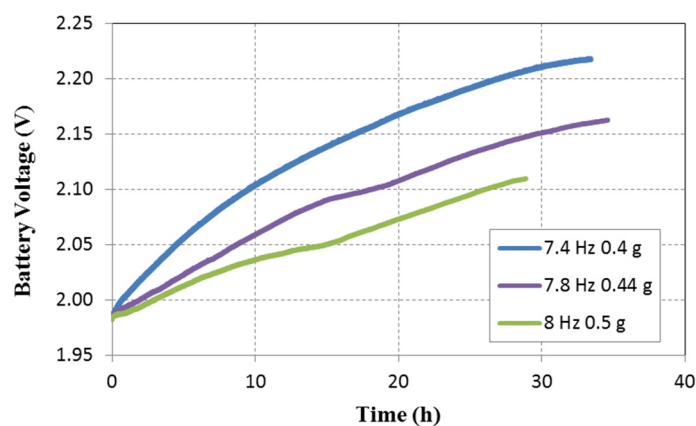


Figure 10 shows the charging profile of the batteries for different vibration conditions. As expected, the energy harvester provides the maximum average charging current of 65 μA to the batteries, when excited at its resonance frequency of 7.4 Hz with 0.4 g peak acceleration. The voltage of the batteries shows a similar trend with different charging durations. However, it takes more than 40 h even for the best case to fully charge the batteries. Therefore, it is more feasible to maintain the fully-charged

batteries at this state with the power delivered by the energy harvester, rather than charging after the battery is depleted. This also enables charging the batteries while they are supplying the specified device, such as the MicaZ mote utilized in this study. This kind of charging is similar to the trickle charging method, due to its small constant charging current rate and its “on-line” charging nature.

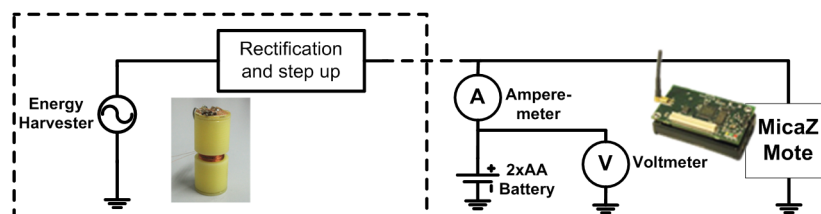
Figure 10. Charging of the two 1800 mA·h batteries in series by the fabricated electromagnetic energy harvester in three different vibration conditions.



4. Energy Harvesting Wireless Sensor Node

Figure 11 presents the test setup for realizing an energy harvesting wireless sensor node. The MicaZ mote was powered by two serially connected rechargeable AA-sized NiMH batteries. Besides, an EM harvester was connected across the batteries for charging. The MicaZ mote was programmed according to the scenario defined in Section 2, for reading the acceleration sensor and transmitting data at different time intervals. The batteries were fully charged at the beginning of the experiment, and the energy harvester was excited with 7.4 Hz and 0.4 g continuous sinusoidal vibration. The same tests were repeated for the case where there is no energy harvester connected, in order to see the contribution of the harvested energy to the battery lifetime. The voltage and the current of the rechargeable battery were continuously measured and recorded during the tests.

Figure 11. Energy harvesting wireless sensor node test setup. The battery voltage and current are measured for two configurations: with and without the inclusion of the energy harvester.



Figures 12–14 show the discharging profiles of the batteries when the MicaZ mote operates with the scenario presented in Section 2.3. The only difference is that three different task execution periods of 1 s, 20 s and 1 min were tested. One of the first observations is that the battery voltage ripples within a band for all of the experiments with and without the energy harvester. This is due to the decreased impedance of the MicaZ mote during the data transmission events: a large current is drawn from the battery when the radio is on.

Figure 12. Discharging profile of the batteries in the operation of the MicaZ mote with a 1-s task execution time; the energy harvester is excited with 7.4 Hz frequency and 0.4 g acceleration.

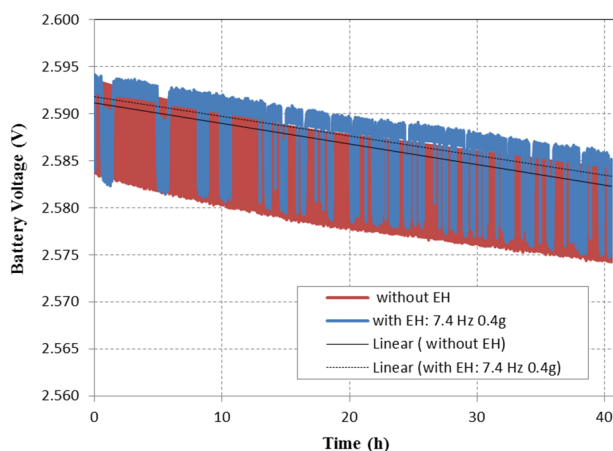


Figure 13. Discharging profile of the batteries in the operation of the MicaZ mote with a 20-s task execution time; the energy harvester is excited with 7.4 Hz frequency and 0.4 g acceleration.

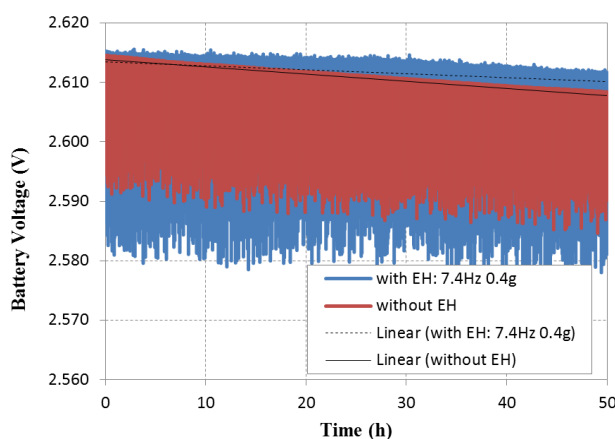
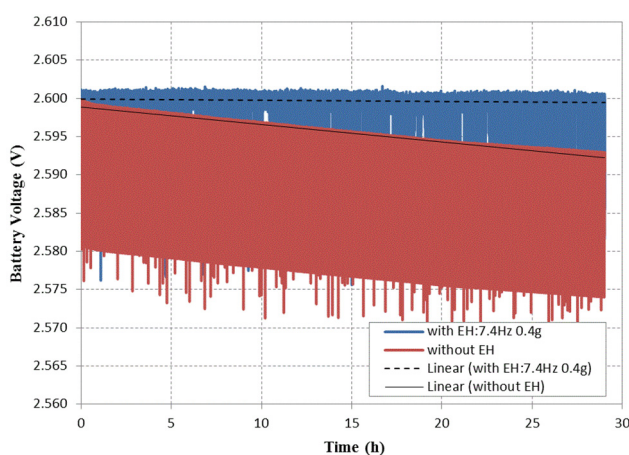


Figure 14. Discharging profile of the batteries in the operation of the MicaZ mote with a 1-min task execution time; the energy harvester is excited with 7.4 Hz frequency and 0.4 g acceleration.



For a 1-s task execution period, Figure 12 depicts that the energy harvester does not have a large impact on the battery voltage and consequently on the battery life. From Figure 13, it is seen that the harvested energy can only replenish the battery discharging for the 20-s task execution period. On the other hand, for the 1-min task execution period case, Figure 14 demonstrates that the harvester almost prevents the batteries from discharging, keeping them in a fully-charged state and guaranteeing node operation at the optimized voltage. The average power consumption of the MicaZ mote for this operation scenario was measured as $186.04 \mu\text{W}$, as presented in Table 2, which means that the energy harvester provides a similar amount of power to the batteries with the given vibration profile.

Comparing the battery voltage trends for different cases (with and without the energy harvester for different task execution periods) shows the significance of adjusting the duty cycle of a wireless sensor node according to the available power generated by the energy harvester. The voltage drop is decreased with an optimized adjustment, increasing the lifetime of the batteries. The voltage drop performance of the batteries is further improved, since the battery charge state is kept close to its maximum capacity in an optimized energy harvesting wireless sensor node.

After this inference, the current across the rechargeable batteries was investigated in detail to get quantitative data on the lifetime of the studied energy harvesting WSN. Figures 15 and 16 show the current drawn from the rechargeable battery during the operation of the MicaZ mote without the energy harvester for task execution periods of 1 s and 1 min. The average current consumption is $255 \mu\text{A}$ and $72 \mu\text{A}$ for the 1-s and 1-min cases, respectively.

Figure 15. The current drawn from the battery in the operation of the MicaZ note (1-s task execution time) without the electromagnetic (EM) energy harvester.

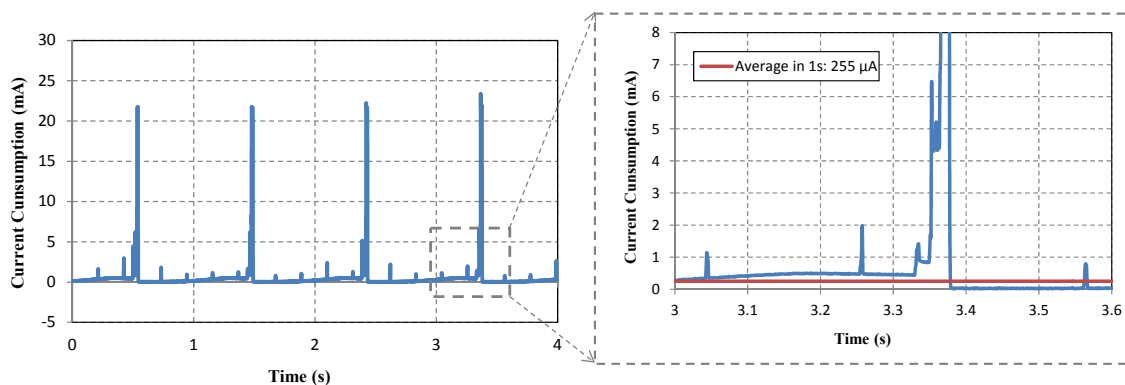
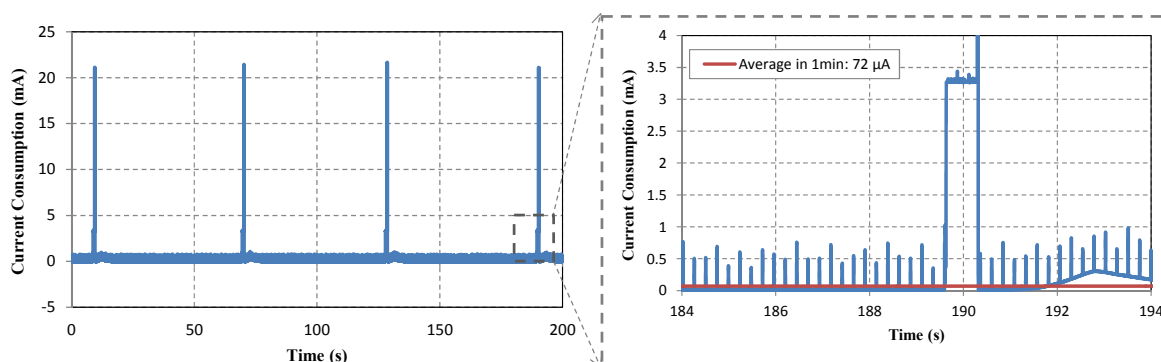


Figure 16. The current drawn from the battery in the operation of the MicaZ note (1-min task execution time) without the EM energy harvester.



On the other hand, Figures 17 and 18 show the battery current with the energy harvester integrated with the system. In this configuration, the energy harvester not only supplies the standby mode current of the MicaZ mote, but it also charges the rechargeable battery during the standby operation. The negative current values seen in Figures 17 and 18 clearly show that the current is forced into the batteries by the energy harvester; therefore, these time slots correspond to the charging instances of the batteries.

Figure 17. The current passing through the rechargeable battery with the 1-s task execution time, when the system operates together with the EM energy harvester.

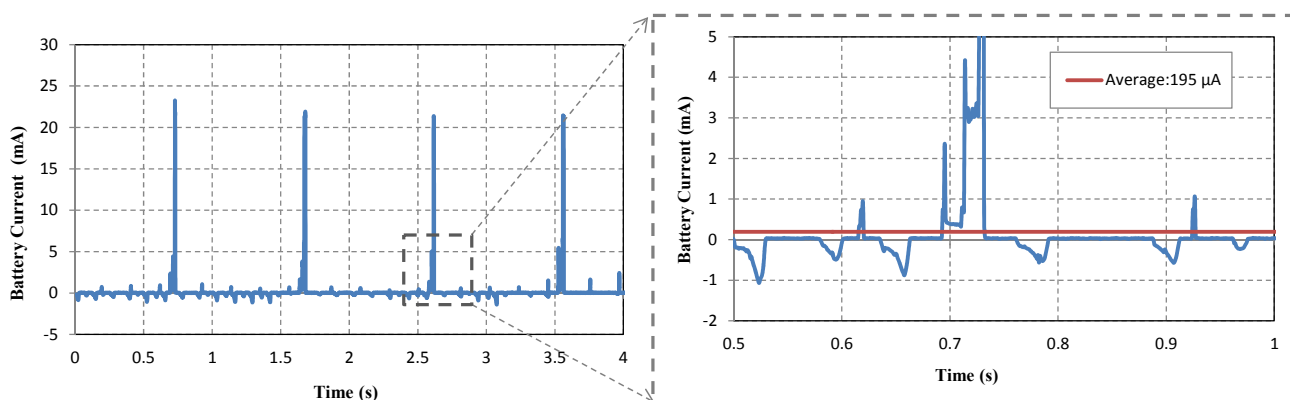


Figure 18. The current passing through the rechargeable battery with the 1-min task execution time, when the system operates together with the EM energy harvester.

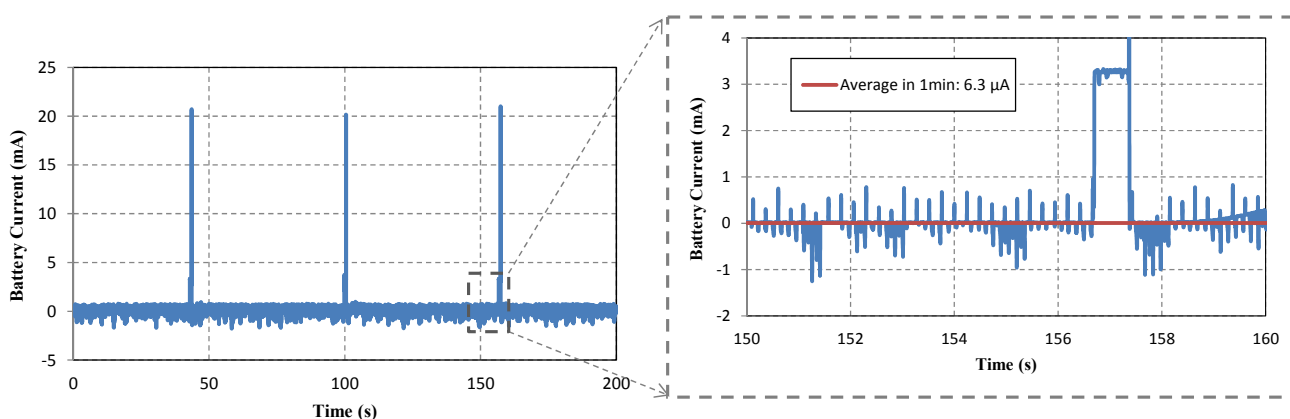


Table 3 presents the average battery current values for different task execution periods and the corresponding expected increase in the battery lifetime. Comparing Figures 15–18, it is seen that the energy harvester saves about $65 \mu\text{A}$ of current from the overall consumption of the system. The average current consumption of the system reduces from $72 \mu\text{A}$ to $6.3 \mu\text{A}$ for the scenario with a 1-min task execution time. This implies that $169 \mu\text{W}$ of power were provided by the energy harvester compared to the dissipated power of $186.04 \mu\text{W}$. This corresponds to 90% of the whole power required by the WSN, resulting in about a 10-times increase in the expected battery lifetime for this scenario.

Table 3. Average battery current and battery lifetime increment.

Task: Read acceleration (10×), average, transmit data execution time	Average current on the batteries		Battery lifetime increment
	Without energy harvester	With energy harvester (7.4 Hz and 0.4 g)	
1 s	255 μ A	195 μ A	30%
20 s	99.7 μ A	38.1 μ A	161%
1 min	72 μ A	6.3 μ A	1042%

Experimental results show that the full capacity of a battery can be maintained through the charging of the energy harvester during the operation of the MicaZ mote, with optimized operation scheduling. Furthermore, the proposed method is also advantageous in terms of battery cycle life, as it provides a low charging current with a maximum peak value of 1 mA. The minimized average current consumption (6.3 μ A) further prolongs the battery lifetime.

5. Conclusions

In this paper, integrating an electromagnetic energy harvester into a WSN node for charging its batteries was demonstrated. The power dissipation of MicaZ motes and the charging and discharging profiles of rechargeable batteries were investigated. It was experimentally shown that the custom-designed EM energy harvester for low frequency vibrations can provide adequate current to charge the batteries of the WSN node and increase its lifetime by a factor of more than 10. The MicaZ sensor node was adjusted for a task operation of reading acceleration sensor data and transmitting it within a 1-min task execution time. Besides, the electromagnetic energy harvester was operated with 7.4 Hz and 0.4 g vibrations. Although the energy harvester cannot supply the required instantaneous power for radio operation (RX or TX), the power demand can be fulfilled by optimizing the operation scheduling and adjusting the duration of the low-power standby mode, creating room for the energy harvester to charge the batteries. Furthermore, integrating an energy harvester into the system is also advantageous in terms of battery cycle life, as it provides a low charging current and minimized average battery current consumption.

The experimental results show that charging rechargeable batteries of a WSN node while it is operational, with an electromagnetic energy harvesting system, is a promising approach for the realization of fully-autonomous sensor networks. The system can be used for offshore environmental monitoring of storms, rain, *etc.*, where the energy source is the ocean waves. Moreover, the system can be used in tunnels or bridges for structural health monitoring by fine tuning the energy harvester resonance frequency according to the environmental vibration conditions, together with a suitable reconfiguration of the MicaZ mote operation.

Acknowledgments

This work is part of the European Coordinated Research on Long-term Challenges in Information and Communication Sciences & Technologies ERA-Net (CHIST-ERA) E-CROPS project, funded by Grant No. 112E175 of the Scientific and Tech. Research Council of Turkey (TUBITAK).

Author Contributions

Salar Chamanian has made contributions on the study of the energy harvesting WSNs and established the test bench and carried out the experiments and results analysis. He also carried out the literature review and prepared manuscript. Sajjad Baghaee has made contributions to the study of MicaZ system and its programming. He has also contributed to the preparation of MicaZ System Architecture and Energy Consumption Features section described in this manuscript. Hasan Ulasan and Ozge Zorlu have made contributions on implementing electromagnetic energy harvesting system. Haluk Hulah and Elif Uysal-Biyikoglu lead the project. Final review, including contents and manuscript editions were done by Haluk Hulah and Elif Uysal-Biyikoglu.

Conflicts of Interest

The authors declare no conflict of interest.

References

1. Gelenbe, E.; Lent, R. Power-aware ad hoc cognitive packet networks. *Ad Hoc Netw.* **2004**, *2*, 205–216.
2. Tekbiyik, N.; Uysal-Biyikoglu, E. Energy efficient wireless unicast routing alternatives for machine-to-machine networks. *J. Netw. Comput. Appl.* **2011**, *34*, 1587–1614.
3. Gelenbe, E.; Gunduz, D. Optimum power level for communications with interference. In Proceedings of the 24th Tyrrhenian International Workshop on Digital Communications-Green ICT (TIWDC), Genoa, Italy, 23–25 September 2013.
4. Gelenbe, E.; Lent, R.; Douratsos, M. Choosing a local or remote cloud. In Proceedings of the Second IEEE Symposium on Network Cloud Computing and Applications NCCA2012, London, UK, 3–5 December 2012.
5. Bacinoglu, B.T.; Uysal-Biyikoglu, E. Finite-horizon online transmission scheduling on an energy harvesting communication link with a discrete set of rates. *J. Commun. Netw.* **2014**, *16*, 300–393.
6. Shakiba-Herfeh, M.; Uysal-Biyikoglu, E. Optimization of feedback in a MISO downlink with energy harvesting users. In Proceedings of the European Wireless 2014, Barcelona, Spain, 14–16 May 2014.
7. Gelenbe, E.; Gesbert, D.; Gunduz, D.; Kulah, H.; Uysal-Biyikoglu, E. Energy harvesting communication networks: Optimization and demonstration (the E-CROPS Project). In Proceedings of the 24th Tyrrhenian International Workshop on Digital Communications-Green ICT (TIWDC), Genoa, Italy, 23–25 September 2013.
8. Guo, W.; Member, S.; Healy, W.M.; Zhou, M. Battery discharge characteristics of wireless sensors in building applications. In Proceedings of the 9th IEEE International Conference on Networking, Sensing and Control (ICNSC), Beijing, China, 11–14 April 2012; pp. 133–138.
9. Rao, R.; Vrudhula, S.; Rakhmatov, D. Battery Modeling for energy aware system design. *Computer* **2003**, *36*, 77–87.
10. Gelenbe, E.; Morfopoulou, C. A framework for energy-aware routing in packet networks. *Comput. J.* **2011**, *54*, 850–859.

11. Alippi, C.; Galperti, C. An adaptive system for optimal solar energy harvesting in wireless sensor network nodes. *IEEE Trans. Circuits Syst. I Regul. Pap.* **2008**, *55*, 1742–1750.
12. Minami, M.; Morito, T. Solar biscuit: A battery-less wireless sensor network system for environmental monitoring applications. In Proceedings of the 2nd International Workshop on Networked Sensing Systems, San Diego, CA, USA, 27–28 June 2005.
13. Barnett, R.E.; Liu, J.; Lazar, S. A RF to DC voltage conversion model for multi-stage rectifiers in UHF RFID transponders. *IEEE J. Solid-State Circuits* **2009**, *44*, 354–370.
14. Scorcioni, S.; Larcher, L. An integrated rf energy harvester for UHF wireless powering applications. In Proceedings of the 2013 IEEE Wireless Power Transfer (WPT), Perugia, Italy, 15–16 May 2013; pp. 92–95.
15. Roundy, S.; Wright, P.K. A piezoelectric vibration based generator for wireless electronics. *Smart Mater. Struct.* **2004**, *13*, 1131–1142.
16. Roundy, S.; Wright, P.K.; Rabaey, J. A study of low level vibrations as a power source for wireless sensor nodes. *Comput. Commun.* **2003**, *26*, 1131–1144.
17. Naruse, Y.; Matsubara, N.; Mabuchi, K.; Izumi, M.; Suzuki, S. Electrostatic micro power generation from low-frequency vibration such as human motion. *J. Micromech. Microeng.* **2009**, *19*, doi:10.1088/0960-1317/19/9/094002.
18. Galchev, T.; Aktakka, E.E.; Kim, H.; Najafi, K. A piezoelectric frequency-increased power generator for scavenging low-frequency ambient vibration. In Proceedings of the IEEE 23rd International Conference on Micro Electro Mechanical Systems, Hong Kong, China, 24–28 January 2010; pp. 1203–1206.
19. Rahimi, A.; Zorlu, O.; Muhtaroglu, A.; Kulah, H. Fully self-powered electromagnetic energy harvesting system with highly efficient dual rail output. *Sens. J. IEEE* **2012**, *12*, 2287–2298.
20. Zhang, S.; Seyedi, A.; Sikdar, B. An analytical approach to the design of energy harvesting wireless sensor nodes. *IEEE Trans. Wirel. Commun.* **2013**, *12*, 4010–4024.
21. Kooti, H.; Dang, N.; Mishra, D.; Bozorgzadeh, E. Energy budget management for energy harvesting embedded systems. In Proceedings of the IEEE 18th International Conference on Embedded and Real-Time Computing Systems and Applications (RTCSA), Seoul, Korea, 19–22 August 2012.
22. Ramachandran, K.; Sikdar, B. A population based approach to model the lifetime and energy distribution in battery constrained wireless sensor networks. *IEEE J. Sel. Areas Commun.* **2010**, *28*, 576–586.
23. Weddell, A.; Grabham, N.; Harris, N.; White, N. Optimal energy management policies for energy harvesting sensor nodes. *IEEE Trans. Wirel. Commun.* **2008**, *9*, 1326–1336.
24. Dondi, D.; Scorcioni, S.; Bertacchini, A.; Larcher, L.; Pavan, P. An autonomous wireless sensor network device powered by a RF energy harvesting system. In Proceedings of the IECON-38th Annual Conference on IEEE Industrial Electronics Society, Montreal, QC, Canada, 25–28 October 2012; pp. 2557–2562.
25. Jang, J.H.; Berdy, D.B.; Lee, J.; Peroulis, D.; Jung, B. A wireless condition monitoring system powered by a Sub-100 μ W vibration energy harvester. *IEEE Trans. Circuits Syst.* **2013**, *60*, 1082–1093.

26. Namboothiri, P.G.; Sivalingam, K.M. Capacity analysis of multi-hop wireless sensor networks using multiple transmission channels: A case study using IEEE 802.15.4 based networks. In Proceedings of the IEEE 35th Conference on Local Computer Networks (LCN), Denver, CO, USA, 10–14 October 2010; pp. 168–171.
27. Crossbow. MTS/MDA Sensor Board Users Manual. Available online: <http://www.xbow.com> (accessed on 10 March 2014).
28. Tinyos.net. TinyOS. Available online: <http://www.tinyos.net> (accessed on 10 March 2014).
29. Baghaee, S.; Gurbuz, S.Z.; Uysal-Biyikoglu, E. Application and modeling of a magnetic WSN for target localization. In Proceedings of the UKSim 15th International Conference on Computer Modelling and Simulation, Cambridge, UK, 10–12 April 2013; pp. 687–692.
30. Crossbow. MPR/MIB User's Manual. Available online: <http://www.xbow.com> (accessed on 10 March 2014).
31. Uluşan, H.; Gharehbaghi, K.; Zorlu, Ö.; Muhtaroglu, A.; Kùlah, H. A fully-integrated and battery-free interface electronics for low voltage electromagnetic energy harvesters. *IEEE Trans. Power Electron.* **2014**, *99*, 1–8.
32. Rahimi, A.; Zorlu, Ö.; Muhtaroglu, A.; Kùlah, H. A compact electromagnetic vibration harvesting system with high performance interface electronics. *Euroensors XXV Procedia Eng.* **2011**, *25*, 215–218.
33. Baghaee, S.; Uluşan, H.; Chamanian, S.; Zorlu, O.; Kulah, H.; Uysal-Biyikoglu, E. Towards a vibration energy harvesting wsn demonstration testbed. In Proceedings of the 24th Tyrrhenian International Workshop on Digital Communications-Green ICT (TIWDC), Genoa, Italy, 23–25 September 2013; pp. 1–6.
34. NXP. PMEG2005EL PMEG2005AEL datasheet. Available online: <http://www.nxp.com> (accessed on 30 January 2014).
35. Energizer.com. Nickel Metal Hydride (NiMH). 7323, 1–16. Available online: <http://www.energizer.com> (accessed on 30 January 2014).

© 2014 by the authors; licensee MDPI, Basel, Switzerland. This article is an open access article distributed under the terms and conditions of the Creative Commons Attribution license (<http://creativecommons.org/licenses/by/4.0/>).